

TRANSONIC AIRFOIL DESIGN BY THE INVERSE METHOD USING VARIABLE-FIDELITY MODELLING

Slawomir Koziel, Leifur Leifsson and Stanislav Ogurtsov
*Engineering Optimization & Modeling Center, School of Science and Engineering
Reykjavik University, Menntavegur 1, Reykjavik, Iceland*

Keywords: Inverse airfoil design, Target pressure distribution, Surrogate models, Variable-resolution modelling, Response surface modelling.

Abstract: The paper presents an improved optimization algorithm for the inverse design of transonic airfoils. Our approach replaces the direct optimization of an accurate, but computationally expensive, high-fidelity airfoil model by an iterative re-optimization of two different surrogate models. Initially, for a few design iterations, a corrected physics-based low-fidelity model is employed, which is subsequently replaced by a response surface approximation model. The low-fidelity model is based on the same governing fluid flow equations as the high-fidelity one, but uses coarser discretization and relaxed convergence criteria. A shape-preserving response prediction technique is utilized to align the pressure distribution of the low-fidelity model with that of the high-fidelity one. This alignment process is particularly suitable since the inverse design aims at matching a given target pressure distribution. Our algorithm is applied to constrained inverse airfoil design in inviscid transonic flow. A comparison with the basic version of the optimization algorithm, exploiting only a physics-based low-fidelity model, is also carried out. While the performance of both versions is similar with respect to their ability to match the target pressure distribution, the improved algorithm offers substantial design cost savings, from 25 to 72 percent, depending on the test case.

1 INTRODUCTION

Aerodynamic shape optimization (ASO) involves the design of aerodynamic components such as aircraft wings and turbine blades (Leoviriyakit et al., 2003); (Braembussche, 2008). The state-of-the-art ASO design methods employ high-fidelity computational fluid dynamic (CFD) simulations as a part of efficient numerical optimization algorithms (Queipo et al., 2005); (Forrester and Keane, 2009); (Alexandrov et al., 2000); (Robinson et al., 2008). The accurate CFD simulations typically lead to more realistic and attainable designs. The downside is that the high-fidelity CFD analysis is computationally expensive and design optimization normally requires a large number of simulations, which leads to a time consuming design process.

The introduction of surrogate-based optimization (SBO) methods (Queipo et al., 2005); (Forrester and Keane, 2009) to ASO permitted reduction of the overall computational cost, as well as handling noisy objective functions. Examples of such work can be found in the literature (see e.g., Alexandrov et al.,

2000); (Robinson et al., 2008); (Booker et al., 1999); (Barrett et al., 2006); (Leifsson and Koziel, 2010); (Lane and Marshall, 2010).

A computationally efficient design optimization methodology for the inverse ASO of transonic airfoils was recently introduced (Leifsson and Koziel, 2011). The approach replaces the direct optimization of an accurate, but computationally expensive, high-fidelity airfoil model by an iterative re-optimization of a corrected low-fidelity model. The low-fidelity model is based on the same governing fluid flow equations as the high-fidelity one, but uses coarser discretization and relaxed convergence criteria. The shape-preserving response prediction technique (Koziel, 2010a) is utilized to align the pressure distribution of the low-fidelity model with that of the high-fidelity model. This alignment process is particularly suitable since a target pressure distribution is specified in the inverse design problem.

In this work, we substantially enhance the optimization methodology introduced in Leifsson and Koziel (2011). More specifically, the low-

fidelity CFD model is replaced - after a few design iterations - by its (local) response surface approximation, which allows us to reduce the overall design cost and obtain faster convergence when compared to the original version of the algorithm. Our approach is demonstrated using several transonic airfoil design cases.

2 PROBLEM FORMULATION

The airfoil shape optimization can be formulated as a constrained nonlinear minimization problem. For a given set of operating conditions, solve

$$\begin{aligned} \min_{\mathbf{x}} f(\mathbf{x}) \quad \text{s.t. } & g_j(\mathbf{x}) \leq 0, j=1, \dots, M; \\ & h_k(\mathbf{x}) = 0, k=1, \dots, N; \mathbf{l} \leq \mathbf{x} \leq \mathbf{u}; \end{aligned} \quad (1)$$

where $f(\mathbf{x})$ is the objective function, \mathbf{x} is the design variable vector, $g_j(\mathbf{x})$ are the inequality constraints, M is the number of the inequality constraints, $h_k(\mathbf{x})$ are the equality constraints, N is the number of the equality constraints, and \mathbf{l} and \mathbf{u} are the design variables lower and upper bounds, respectively.

There are two main approaches to airfoil design. One is to directly adjust the geometry parameters of the airfoil section in order to maximize its performance. This is called direct design, and the most common formulations include lift maximization, drag minimization, and lift-to-drag ratio maximization (Leifsson and Kozel, 2010). Another way is to define a priori a specific flow behavior that is to be attained. The airfoil shape is then designed to achieve this flow behavior. This is called inverse design (Dulikravich, 1991).

In inverse design, the role of the designer is to specify a particular flow feature, which typically is a target pressure distribution, $C_{p,t}$, on the surface of the airfoil. The task is then to find the airfoil shape that can give the target pressure distribution at the desired flow condition. This can be done by minimizing the difference between the pressure distribution of the airfoil C_p and the target distribution $C_{p,t}$.

The objective function can be formulated as the L^2 norm of the difference between the airfoil pressure distribution and the target pressure distribution, or $f(\mathbf{x}) = \frac{1}{2} \int [C_p(\mathbf{x}) - C_{p,t}]^2 ds$. A minimum thickness is normally specified so that the optimizer does not reduce the airfoil to a thin plate. The thickness constraint can be written as $g(\mathbf{x}) = A_{min} - A(\mathbf{x}) \leq 0$, where $A(\mathbf{x})$ is the cross-sectional area of the airfoil and A_{min} is the minimum cross-sectional area.

In this paper, we use the NACA airfoil shapes. In

particular, we use the NACA four-digit airfoil parameterization method, where the airfoil shape is defined by three parameters m (the maximum ordinate of the mean camberline as a fraction of chord), p (the chordwise position of the maximum ordinate) and t/c (the thickness-to-chord ratio). The airfoils are denoted by NACA $mpxx$, where xx represents the value of t/c . The shapes are constructed using two polynomials, one for the thickness distribution and the other for the mean camber line. The full details of the NACA four-digit parameterization method are given in Abbott and Doenhoff (1959). Three example NACA four-digit airfoils are shown in Fig. 1.

3 CFD MODELLING

A single CFD simulation is, in general, composed of four steps; the geometry generation (described here in Section 2), meshing of the solution domain, numerical solution of the governing fluid flow equations, and post-processing of the flow results, which involves, in the case of numerical optimization, calculating the objectives and constraints. In this section we present the high- and low-fidelity CFD models.

3.1 High-fidelity CFD Model

The flow is assumed to be steady, inviscid, and adiabatic with no body forces. The Euler equations are taken to be the governing fluid flow equations (Tannehill et al., 1997). The computational meshes used in this study are all of structured curvilinear body-fitted C-topology.

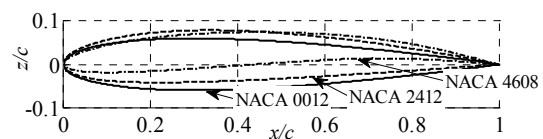


Figure 1: Shown are three different NACA four-digit airfoil sections; NACA 0012 ($m = 0, p = 0, t/c = 0.12$) solid line (-), NACA 2412 ($m = 0.02, p = 0.4, t/c = 0.12$) dashed line (--), NACA 4608 ($m = 0.04, p = 0.6, t/c = 0.08$) dash-dot line (-.-).

The solution domain boundaries are placed at 24 chord lengths in front of the airfoil, 50 chord lengths behind it, and 25 chord lengths above and below it. The meshes are generated with the computer code ICFM CFD (2006). A fine mesh was developed with a total of 320 points in the vertical direction, 180 points on the airfoil surface and 160 points in the

wake behind the airfoil, with a total of 106 thousand cells. An example computational mesh is shown in Fig. 2.

The numerical fluid flow simulations are performed using the computer code FLUENT (2006). Asymptotic convergence to a steady state solution is obtained for each case. The iterative convergence of each solution is examined by monitoring the overall residual, which is the sum (over all the cells in the computational domain) of the L^2 norm of all the governing equations solved in each cell. In addition to this, the lift and drag forces (defined in Section 3.3) are monitored for convergence. The criteria used in this work for the high-fidelity model is a maximum residual of 10^{-6} , or a maximum number of iterations of 1000.

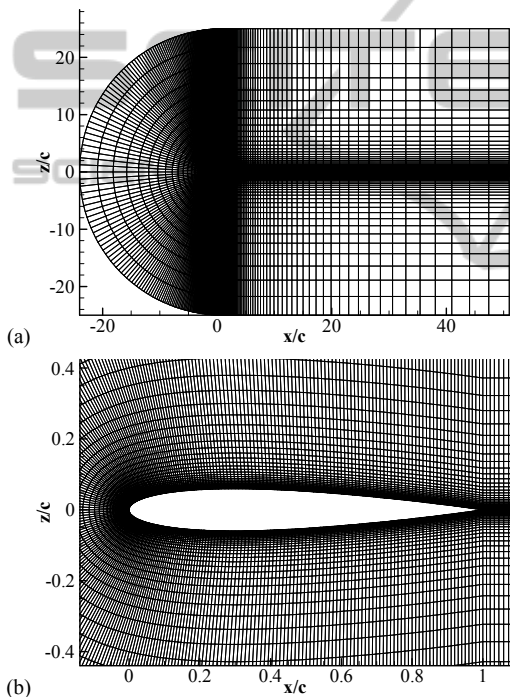


Figure 2: (a) An example computational mesh with a structured C-topology for a NACA 0012 airfoil; (b) a view close to the airfoil surface.

3.2 Low-fidelity CFD Model

The low-fidelity CFD model is constructed using the high-fidelity model, but with a coarser computational mesh and relaxed convergence criteria. The parameters of the mesh and the number of solver iterations were obtained by performing a parametric study using the NACA 2412 airfoil section at $M_\infty = 0.75$ and $\alpha = 1$ deg.

Initially the fine mesh is solved to full convergence. The solver needed 216 iterations to

reach a converged solution based on the residuals of the governing equations. However, the lift and drag coefficient values reached a converged value after approximately 50 iterations. Therefore, the number of iterations limit was set to 100 hundred iterations in the subsequent steps.

The mesh points were reduced in two steps. First, the number of mesh points in the z -direction and the number of mesh points behind the airfoil were reduced by (approximately) half. This procedure was repeated and in each step the pressure distribution was plotted. It was observed that the shock location moved rearward. After five subsequent steps, the pressure distribution became highly distorted near the leading-edge. The previous mesh was then retained and the number of mesh points on the airfoil surface was reduced incrementally. Again, the pressure distribution was plotted for each step. It was observed that the shock strength reduced in each step as the mesh got coarser and coarser on the airfoil surface. After three steps the procedure was halted. The resulting mesh has 48 points in the z -direction, 115 points on the airfoil surface, and 20 points in the wake behind the airfoil, with a total of 8295 thousand cells. The overall evaluation time is reduced to about 34 s, which is approximately 13.5 times faster than the high-fidelity model using the fine mesh and traditional convergence criteria.

The overall evaluation time of the high-fidelity model in this parametric study is 471 s with a total of 216 iterations. In many cases the solver does not fully converge with respect to the residuals and goes on up to 1000 iterations. Then the overall evaluation time goes up to 2500 s, and the low-fidelity model is approximately 73 times faster. For the sake of simplicity, we will use a fixed value of 50 in the numerical computations presented later in the paper.

3.3 Aerodynamic Forces

The non-dimensional force coefficients parallel to the x - and z -axes, C_x and C_z , respectively, are calculated by integrating the pressure distribution C_p over the surface of the airfoil as (Tannehill et al., 1997)

$$C_x = \oint C_p \sin \theta \, ds, \quad C_z = -\oint C_p \cos \theta \, ds \quad (2)$$

where ds is the surface panel element of length and θ is the angle the panel makes relative to the x -axis. The lift coefficient C_l and the wave drag coefficient C_{dw} are calculated as

$$\begin{aligned} C_l &= -C_x \sin \alpha + C_z \cos \alpha, \\ C_{dw} &= C_x \cos \alpha + C_z \sin \alpha. \end{aligned} \quad (3)$$

4 SURROGATE MODELING

In order to use the low-fidelity model as a reliable prediction tool in the optimization process, it has to be corrected to become a reliable representation of the high-fidelity model. The corrected low-fidelity model is called a surrogate. The surrogate model can replace the high-fidelity one in the optimization process and thus reduce the overall optimization cost.

Here, we adopt a shape-preserving response prediction (SPRP) methodology introduced in (Koziel, 2010a) in the context of microwave engineering, and recently applied for direct airfoil design (Leifsson and Koziel, 2010). SPRP is easy to implement, unlike space mapping it does not need any auxiliary transformations or extractable parameters (Koziel et al., 2008). Also, it does not require high-fidelity model derivative information.

By formulation, SPRP works directly with the model outputs that can be described by certain number of design-variable-dependent characteristic features (Koziel, 2010a). In the case of a pressure distribution, these features may include the location and strength of the shock, the pressure at the leading- and trailing-edges, and many others. In direct airfoil design, the pressure distribution is an intermediate simulation result, with the figures of interest, such as lift or wave drag, being derived from it. In inverse design, the pressure distribution is the main object of interest, which makes SPRP well suited for this kind of problem.

We will denote the vector of design variables as \mathbf{x} . The pressure distribution for the high- and low-fidelity models will be denoted as $C_{p,f}$ and $C_{p,c}$, respectively. The surrogate model is constructed assuming that the change of $C_{p,f}$ due to the adjustment of the design variables \mathbf{x} can be predicted using the actual changes of $C_{p,c}$. The change of $C_{p,c}$ is described by the translation vectors corresponding to certain (finite) number of its characteristic points. These translation vectors are subsequently used to predict the change of $C_{p,f}$, whereas the actual $C_{p,f}$ at the current design, $C_{p,f}(\mathbf{x}^{(i)})$, is treated as a reference.

Figure 3(a) shows the pressure distribution $C_{p,c}$ of the low-fidelity model at $\mathbf{x}^{(i)} = [0.02 \ 0.4 \ 0.12]^T$ (NACA 2412 airfoil) for $M_\infty = 0.7$ and $\alpha = 1$ deg, as well as $C_{p,c}$ at $\mathbf{x} = [0.025 \ 0.56 \ 0.122]^T$; $\mathbf{x}^{(i)}$ will denote a current design (at the i th iteration of the optimization algorithm; the initial design will be denoted as $\mathbf{x}^{(0)}$ accordingly). Circles denote characteristic points of $C_{p,c}(\mathbf{x}^{(i)})$, here, representing, among others, x/c equal to 0 and 1 (leading and trailing airfoil edges, respectively), the maxima of

$C_{p,c}$ for the lower and upper airfoil surfaces, as well as the local minimum of $C_{p,c}$ for the upper surface. The last two points are useful to locate the pressure shock. Squares denote corresponding characteristic points for $C_{p,c}(\mathbf{x})$, while small line segments represent the translation vectors that determine the “shift” of the characteristic points of $C_{p,c}$ when changing the design variables from $\mathbf{x}^{(i)}$ to \mathbf{x} .

In order to obtain a reliable prediction, the number of characteristic points has to be larger than illustrated in Fig. 3(a). Additional points are inserted in between initial points either uniformly with respect to x/c (for those parts of the pressure distribution that are almost flat) or based on the relative pressure value with respect to corresponding initial points (for those parts of the pressure distribution that are “steep”). Figure 3(b) shows the full set of characteristic points (initial points are distinguished using larger markers).

The pressure distribution of the high-fidelity model at the given design, here, \mathbf{x} , can be predicted using the translation vectors applied to the corresponding characteristic points of the pressure distribution of the high-fidelity model at $\mathbf{x}^{(i)}$, $C_{p,f}(\mathbf{x}^{(i)})$. This is illustrated in Figure 4(a) where only initial characteristic points and translation vectors are shown for clarity. Figure 4(b) shows the predicted pressure distribution of the high-fidelity model at \mathbf{x} as well as the actual $C_{p,f}(\mathbf{x})$. The agreement between both curves is very good.

Rigorous formulation of the SPRP technique can be found in Koziel (2010a). We omit the details here for the sake of brevity. It should be mentioned that the SPRP model assumes that the high- and low-fidelity model pressure distributions have corresponding sets of characteristic points. This is usually the case for the practical ranges of design variables because the overall shape of the distributions is similar for both models. In case of a lack of correspondence, original definitions of characteristic points are replaced by their closest counterparts. The typical example would be non-existence of the local minimum of the pressure distribution for the upper surface for the high- and/or low-fidelity model at certain designs. In this case, the original point (local minimum) is replaced by the points characterized by the largest curvature.

5 OPTIMIZATION PROCEDURE

5.1 Objective Function

In inverse design, the primary objective is the align-

ment between the pressure distribution of the airfoil being designed and the prescribed target. The alignment can be measured using a norm.

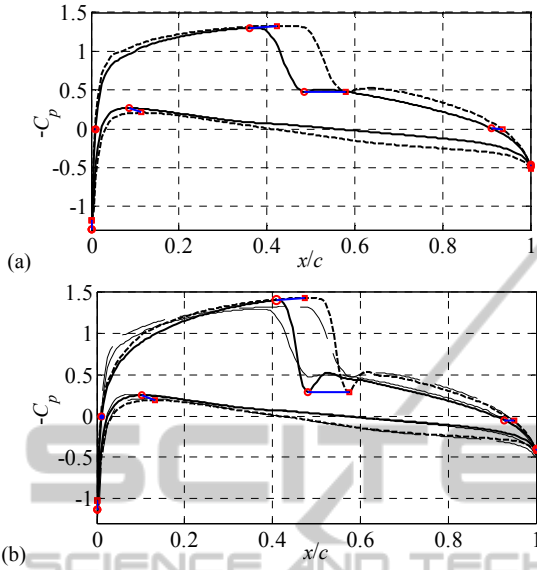


Figure 3: (a) Example low-fidelity model pressure distribution at the design $x^{(i)}$, $C_{p,c}(x^{(i)})$ (solid line), the low-fidelity model pressure distribution at other design x , $C_{p,c}(x)$ (dotted line), characteristic points of $C_{p,c}(x^{(i)})$ (circles) and $C_{p,c}(x)$ (squares), and the translation vectors (short lines); (b) low-fidelity model pressure distributions, initial characteristic points (large markers) and translation vectors from Fig. 3(a) as well as additional points (small markers) inserted in between the initial points either uniformly with respect to x/c (for those parts of the pressure distribution that are almost flat) or based on the relative pressure value with respect to corresponding initial points (for those parts of the pressure distribution that are “steep”).

Due to unavoidable misalignment between the pressure distributions of the high-fidelity model and its SPRP surrogate, it is not convenient to use some of the constraints (e.g., a maximum allowable drag) directly. This is because the design that is feasible for the surrogate model, may not be feasible for the high-fidelity model. In particular, the design obtained as a result of optimizing the surrogate model $C_{p,s}^{(i)}$, i.e., $\mathbf{x}^{(i+1)}$, will be feasible for $C_{p,s}^{(i)}$. However, if $\mathbf{x}^{(i+1)}$ is not feasible for the high-fidelity model, it will not be feasible for $C_{p,s}^{(i+1)}$ because we have $C_{p,s}^{(i+1)}(\mathbf{x}^{(i+1)}) = C_{p,f}(\mathbf{x}^{(i+1)})$ by the definition of the surrogate model. In order to alleviate this problem, we shall use the penalty function approach to handle the drag constraint. Of course, this does not apply to constraints that depend exclusively on the airfoil geometry, such as the minimum airfoil cross-sectional area.

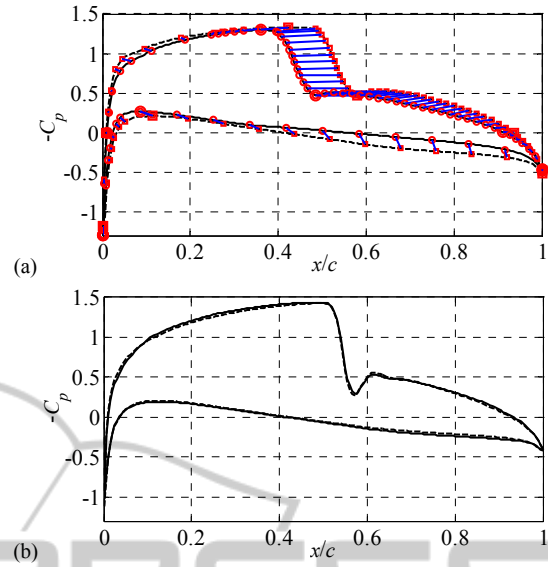


Figure 4: (a) High-fidelity model pressure distribution at $x^{(i)}$, $C_{p,f}(x^{(i)})$ (solid line) and the predicted high-fidelity model C_p at x (dotted line) obtained using SPRP based on characteristic points of Fig. 3(b); characteristic points of $C_{p,f}(x^{(i)})$ (circles) and the translation vectors (short lines) were used to find the characteristic points (squares) of the predicted high-fidelity model pressure distribution (only initial points are shown for clarity); low-fidelity model distributions $C_{p,c}(x^{(i)})$ and $C_{p,c}(x)$ are plotted using thin solid and dotted line, respectively; (b) high-fidelity model pressure distribution at x , $C_{p,f}(x)$ (solid line), and the predicted high-fidelity model pressure distribution at x obtained using SPRP (dotted line).

In this work, all the constraints are handled through penalty functions so that the objective function is defined as follows

$$H(C_p(\mathbf{x})) = F^2 + \beta [\Delta C_{dw,s}(C_p(\mathbf{x}))]^2 + \delta [\Delta C_{l,s}(C_p(\mathbf{x}))]^2 + \gamma [\Delta A(\mathbf{x})]^2 \quad (4)$$

with $F = \|C_p(\mathbf{x}) - C_{p,t}\|$, where $C_{p,t}$ is the target pressure distribution, $\Delta C_{dw,s} = 0$ if $C_{dw,s} \leq C_{dw,s,max}$ and $\Delta C_{dw,s} = C_{dw,s} - C_{dw,s,max}$ otherwise, $\Delta C_{l,s} = 0$ if $C_{l,s} \geq C_{l,s,min}$ and $\Delta C_{l,s} = C_{l,s} - C_{l,s,min}$ otherwise, and $\Delta A = 0$ if $A \geq A_{min}$ and $\Delta A = A - A_{min}$ otherwise. In our numerical experiments we use $\beta = \delta = \gamma = 1000$. Here, the pressure distribution for the surrogate model is $C_p = C_{p,s}$, and for the high-fidelity model $C_p = C_{p,f}$. Also, $C_{l,s}$ and $C_{dw,s}$ denote the lift and wave drag coefficients (both being functions of the pressure distribution).

5.2 Basic Optimization Algorithm

The basic optimization algorithm (Leifsson and

Koziel, 2011) exploits the SPRP-based surrogate model and a trust-region convergence safeguard (Conn et al., 2000). It can be summarized as follows:

1. Set $i = 0$; Select λ (initial trust region radius); Evaluate $C_{p,f}(\mathbf{x}^{(0)})$;
2. Set up SPRP model;
3. Obtain $\mathbf{x}^{(i+1)} = \operatorname{argmin}\{l \leq \mathbf{x} \leq u, \|\mathbf{x} - \mathbf{x}^{(i)}\| \leq \lambda : H(C_{p,s}^{(i)}(\mathbf{x}))\}$;
4. Evaluate high-fidelity model to get $C_{p,f}(\mathbf{x}^{(i)})$;
5. If $H(C_{p,f}^{(i)}(\mathbf{x}^{(i+1)})) < H(C_{p,f}^{(i)}(\mathbf{x}^{(i)}))$ accept $\mathbf{x}^{(i+1)}$; Otherwise $\mathbf{x}^{(i+1)} = \mathbf{x}^{(i)}$;
6. Update λ ;
7. Set $i = i + 1$;
8. If termination condition is not satisfied, go to 2.
9. END

The SPRP surrogate model is updated before each iteration of the optimization algorithm using the high-fidelity model data at the design obtained in the previous iteration. The trust-region parameter λ is updated after each iteration, i.e., decreased if the new design was rejected or if the improvement of the high-fidelity model objective function was too small compared to the prediction given by the SPRP surrogate, or increased otherwise. We use classical updating rules (Conn et al., 2000; Koziel et al., 2006). The algorithm is terminated if $\|\mathbf{x}^{(i+1)} - \mathbf{x}^{(i)}\| < 0.001$ or $\lambda < 0.001$.

5.3 Improved Optimization Scheme

In algorithm of Section 5.2, the new solution $\mathbf{x}^{(i+1)}$ is obtained by optimizing the SPRP model, which involves multiple evaluations of the low-fidelity model. In our case, the low-fidelity model is about 50 times faster than the high-fidelity one, and a typical surrogate model optimization requires 50 to 100 low-fidelity model calls. Thus, the low-fidelity model evaluations are responsible for about 50 to 70 percent of the total optimization cost.

In this section, we formulate the improved optimization scheme that aims at reducing the aforementioned computational overhead. The idea is to replace the low-fidelity model—at some point during the optimization run—by its response surface approximation model. This replacement is executed if $\|C_{p,c}(\mathbf{x}^{(i-1)}) - C_{p,c}(\mathbf{x}^{(i)})\| < \varepsilon_{\max}$ where ε_{\max} is a user-defined threshold value (here, we use $\varepsilon_{\max} = 0.05$). This allows us to avoid constructing the response surface model in the entire design space (which would be too expensive in terms of the number of necessary data points), but only in the vicinity of the current solution $\mathbf{x}^{(i)}$. In this work, we use kriging

interpolation (Queipo et al., 2005) as the response surface model. The model is set up using $N_{kr} = 20$ low-fidelity model evaluations allocated—using Latin Hypercube Sampling (Beachkofski and Grandhi, 2002)—in the interval $[\mathbf{x}^{(i)} - \boldsymbol{\delta}_{kr}, \mathbf{x}^{(i)} + \boldsymbol{\delta}_{kr}]$, where $\boldsymbol{\delta}_{kr} = [0.001 \ 0.04 \ 0.005]^T$.

The improved algorithm can be summarized as follows:

1. Set $i = 0$; Select λ (initial trust region radius); Set the model selector $L = 0$; Evaluate $C_{p,f}(\mathbf{x}^{(0)})$;
2. If $L = 0$ set up SPRP model using the low-fidelity model; Otherwise, set up SPRP model using the kriging model of $C_{p,c}$;
3. Obtain $\mathbf{x}^{(i+1)} = \operatorname{argmin}\{l \leq \mathbf{x} \leq u, \|\mathbf{x} - \mathbf{x}^{(i)}\| \leq \lambda : H(C_{p,s}^{(i)}(\mathbf{x}))\}$;
4. Evaluate high-fidelity model to get $C_{p,f}(\mathbf{x}^{(i)})$;
5. If $H(C_{p,f}^{(i)}(\mathbf{x}^{(i+1)})) < H(C_{p,f}^{(i)}(\mathbf{x}^{(i)}))$ accept $\mathbf{x}^{(i+1)}$; Otherwise $\mathbf{x}^{(i+1)} = \mathbf{x}^{(i)}$;
6. Update λ ;
7. Set $i = i + 1$;
8. If $L = 0$ and $\|C_{p,c}(\mathbf{x}^{(i-1)}) - C_{p,c}(\mathbf{x}^{(i)})\| < \varepsilon_{\max}$, set $L = 1$ and set up the kriging model of $C_{p,c}$ in the interval $[\mathbf{x}^{(i)} - \boldsymbol{\delta}_{kr}, \mathbf{x}^{(i)} + \boldsymbol{\delta}_{kr}]$;
9. If termination condition is not satisfied, go to 2.
10. END

In practice (cf. Section 6), the condition $\|C_{p,c}(\mathbf{x}^{(i-1)}) - C_{p,c}(\mathbf{x}^{(i)})\| < \varepsilon_{\max}$ is satisfied after one or two iterations which allows us to substantially reduce the number of low-fidelity model evaluations in the optimization process.

6 NUMERICAL EXAMPLES

6.1 General Setup

The proposed optimization method is applied to the inverse design optimization of four cases. Designs are obtained using the basic algorithm in Section 5.2, and the improved algorithm in Section 5.3. The surrogate model optimization is performed using the pattern-search algorithm (Koziel, 2010b). For comparison purposes, designs obtained through direct optimization of the high-fidelity model using the pattern-search algorithm (Koziel, 2010b) are also presented.

The design variables are the airfoil shape parameters in the NACA four-digit parameterization (Section 2), i.e., $\mathbf{x} = [m \ p \ t]^T$. Note that the chord length is set to 1. The only inequality constraint is the minimum cross-sectional area constraint. There

are no equality constraints. The side constraints are $0 \leq m \leq 0.1$, $0.2 \leq p \leq 0.8$, and $0.05 \leq t \leq 0.20$. The test cases were chosen only for verification purposes and they do not represent optimal airfoil designs.

6.2 Results of Case Studies

The numerical results of the case studies are presented in Table 1. The target pressure distribution is the same for cases 1, 2, and 3, i.e., $\mathbf{x} = [0.0163 \ 0.4004 \ 0.1118]^T$ with $M_\infty = 0.75$ and $\alpha = 0^\circ$. In case 1 the initial design is NACA 2412 and $A_{min} = 0.078$. For case 1, both the basic and the improved algorithms hit the cross-sectional area constraint and match the target pressure distribution only relatively closely ($F = 0.0243$ and $F = 0.0246$, respectively). However, the improved algorithm requires 5 equivalent high-fidelity model evaluations, while the basic algorithm needs 18. The direct optimization of the high-fidelity model required 201 model evaluations.

In case 2, the constraint value is lowered to $A_{min} = 0.075$, while keeping other parameters the same. Now the algorithms are able to match the target distribution much closer ($F = 0.0025$ and $F = 0.0011$, respectively) with the design cost of about 13 equivalent high-fidelity function calls for the basic algorithm, and 5 for the improved version. Figure 5 shows the pressure distributions of the initial and optimized designs. The high-fidelity CFD model and the pattern-search algorithm required 152 model evaluations.

Table 1: Numerical results of four inverse design case studies using the proposed optimization methodology. F is the norm of the difference of pressure distributions for the optimized and the target designs. N_c is the number of low-fidelity model evaluations and N_f is the number of high-fidelity model evaluations. All the numerical values are from the high-fidelity model.

Case 1					
$M_\infty = 0.75, \alpha = 0^\circ, A_{min} = 0.078$					
Variable	Initial	Target	Pattern-Search [#]	SPRP [§]	Improved SPRP [%]
M	0.0200	0.0163	0.0153	0.0154	0.0155
P	0.4000	0.4004	0.4089	0.4043	0.3985
T	0.1200	0.1118	0.1159	0.1158	0.1159
C_l	0.4745	0.3832	0.3663	0.3663	0.3671
C_{dv}	0.0115	0.0049	0.0049	0.0050	0.0052
A	0.0808	0.0753	0.0780	0.0780	0.0781
F	N/A	N/A	0.0249	0.0243	0.0246
N_c	N/A	N/A	0	330	70
N_f	N/A	N/A	201	11	3
Total cost*	N/A	N/A	201	< 18	< 5

Case 2					
$M_\infty = 0.75, \alpha = 0^\circ, A_{min} = 0.075$					
Variable	Initial	Target	Pattern-Search [#]	SPRP [§]	Improved SPRP [%]
M	0.0200	0.0163	0.0162	0.0162	0.0163
P	0.4000	0.4004	0.4007	0.4014	0.4011
T	0.1200	0.1118	0.1122	0.1121	0.1119
C_l	0.4745	0.3832	0.3816	0.3822	0.3829
C_{dv}	0.0115	0.0049	0.0049	0.0048	0.0049
A	0.0808	0.0753	0.0756	0.0755	0.0753
F	N/A	N/A	0.0025	0.0025	0.0011
N_c	N/A	N/A	0	240	70
N_f	N/A	N/A	152	8	3
Total cost*	N/A	N/A	152	< 13	< 5

Case 3					
$M_\infty = 0.75, \alpha = 0^\circ, A_{min} = 0.075$					
Variable	Initial	Target	Pattern-Search [#]	SPRP [§]	Improved SPRP [%]
m	0.0000	0.0163	0.0156	0.0163	0.0161
p	0.5000	0.4004	0.4252	0.3978	0.4030
t	0.1000	0.1118	0.1139	0.1117	0.1126
C_l	0.0005	0.3832	0.3776	0.3835	0.3801
C_{dv}	0.0002	0.0049	0.0045	0.0049	0.0048
A	0.0673	0.0753	0.0767	0.0752	0.0758
F	N/A	N/A	0.0181	0.0023	0.0048
N_c	N/A	N/A	0	468	70
N_f	N/A	N/A	201	6	5
Total cost*	N/A	N/A	201	< 16	< 7

Case 4					
$M_\infty = 0.75, \alpha = 1^\circ, A_{min} = 0.065$					
Variable	Initial	Target	Pattern-Search [#]	SPRP [§]	Improved SPRP [%]
m	0.0000	0.0300	0.0287	0.0293	0.0300
p	0.4000	0.2000	0.2067	0.2057	0.2000
t	0.1200	0.1000	0.1083	0.1022	0.1000
C_l	0.2082	0.8035	0.7786	0.7905	0.8034
C_{dv}	0.0024	0.0410	0.0424	0.0405	0.0410
A	0.0808	0.0675	0.0731	0.0689	0.0675
F	N/A	N/A	0.0492	0.0182	0.00097
N_c	N/A	N/A	0	457	120
N_f	N/A	N/A	202	6	9
Total cost*	N/A	N/A	202	< 16	< 12

[#] Design obtained using the high-fidelity model and the grid-search algorithm (Koziel, 2010b).

[§] Design obtained using the basic algorithm of Section 5.2; surrogate model optimization performed using the grid-search algorithm (Koziel, 2010b).

[%] Design obtained using the improved algorithm proposed in Section 5.3; surrogate model optimization performed using the grid-search algorithm (Koziel, 2010b).

* The total optimization cost is expressed in terms of the equivalent number of high-fidelity model evaluations. The ratio of the high-fidelity model evaluation time to the corrected low-fidelity model evaluation time varies between 13.5 to 73 depending on the design. For the sake of simplicity we use a fixed value of 50 here.

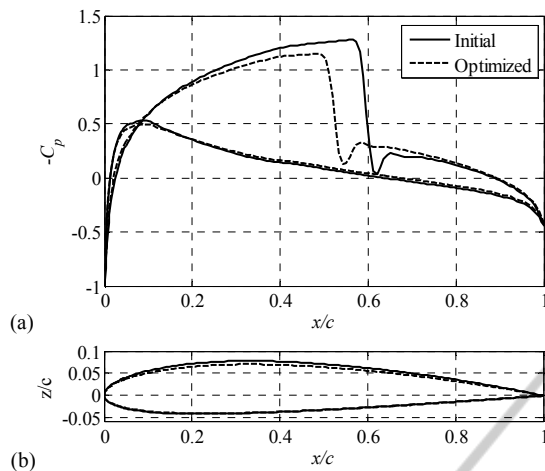


Figure 5: The pressure distributions and airfoil shapes for the initial and optimized designs for case 2.

Case 3 starts with a different initial design, namely, the NACA 0010. Here, both algorithms match the target closely. The basic algorithm requires 16 equivalent high-fidelity function calls, whereas the improved algorithm 7.

In case 4, the target pressure distribution is the one of NACA 3210 at $M_\infty = 0.75$ and $\alpha = 1^\circ$. The initial design is NACA 0012 and the minimum cross-sectional area is $A_{min} = 0.065$. The improved algorithm is able to match the target closely in less than 12 equivalent high-fidelity model evaluations. The basic algorithm and the direct pattern-search are both unable to match the target closely.

7 CONCLUSIONS

Computationally efficient variable-fidelity design of transonic airfoils is presented. The algorithm replaces the direct optimization of a CPU-intensive high-fidelity CFD model by iterative updating and re-optimization of its fast surrogate. The surrogate is constructed using a shape-preserving response prediction technique with the underlying low-fidelity CFD model, which is replaced—after a few iterations—by its local response surface approximation. The operation and performance of our algorithm is demonstrated using several transonic airfoil design cases with the optimized designs obtained at a low cost corresponding to a few high-fidelity CFD simulations. Our results indicate that the algorithm presented here is computationally much more efficient than its basic version that only exploits the corrected CFD low-fidelity model but not the response surface one.

REFERENCES

- Abbott, I. H., and Von Doenhoff, A. E., 1959, *Theory of Wing Sections*, Dover Publications, 1959.
- Alexandrov, N. M., Lewis, R. M., Gumbert, C. R., Green, L. L., and Newman, P. A., 2000, Optimization with Variable-Fidelity Models Applied to Wing Design, *38th Aerospace Sciences Meeting & Exhibit*, Reno, NV, AIAA Paper 2000-0841.
- Barrett, T. R., Bressloff, N. W., and Keane, A. J., 2006, Airfoil Design and Optimization Using Multi-Fidelity Analysis and Embedded Inverse Design, AIAA Paper 2006-1820, *47th AIAA/ASME/ASCE/AHS/ASC Structures, Structural Dynamics, and Materials Conference*, Newport, Rhode Island.
- Beachkofski B. and Grandhi R., 2002. Improved distributed hypercube sampling. *American Institute of Aeronautics and Astronautics*, paper AIAA 2002-1274.
- Booker, A.J., Dennis Jr., J.E., Frank, P.D., Serafini, D.B., Torczon, V., and Trosset, M.W., 1999, A rigorous framework for optimization of expensive functions by surrogates, *Structural Optimization*, vol. 17, no. 1, pp. 1-13.
- Braembussche, R. A., 2008, Numerical Optimization for Advanced Turbomachinery Design, In *Optimization and Computational Fluid Dynamics*, Thevenin, D. and Janiga, G., editors, Springer, pp. 147-189.
- Conn, A. R., Gould, N. I. M., and Toint, P. L., 2000, *Trust Region Methods*, MPS-SIAM Series on Optimization.
- Dulikravich, G. S., 1991, Aerodynamic Shape Design and Optimization, *29th AIAA Aerospace Sciences Meeting*, Reno, NV.
- FLUENT, ver. 12.1, ANSYS Inc., Southpointe, 275 Technology Drive, Canonsburg, PA 15317, 2006.
- Forrester, A. I. J., and Keane, A. J., 2009, Recent advances in surrogate-based optimization, *Progress in Aerospace Sciences*, vol. 45, no. 1-3, pp. 50-79.
- ICEM CFD, ver. 12.1, ANSYS Inc., Southpointe, 275 Technology Drive, Canonsburg, PA 15317, 2006.
- Koziel, S., Bandler, J. W., and Madsen, K., 2006, Space-mapping based interpolation for engineering optimization. *IEEE Trans. Microwave Theory and Tech.*, 54 (6), pp. 2410-2421.
- Koziel, S., Cheng, Q. S., and Bandler, J. W., 2008, Space mapping, *IEEE Microwave Magazine*, vol. 9, no. 6, pp. 105-122.
- Koziel, S., 2010a, Shape-preserving response prediction for microwave design optimization, *IEEE Trans. Microwave Theory and Tech.*, vol. 58, pp. 2829-2837.
- Koziel, S., 2010b, Multi-fidelity multi-grid design optimization of planar microwave structures with Sonnet. *International Review of Progress in Applied Computational Electromagnetics*, Tampere, Finland, pp. 719-724.
- Labrujere, T. E. and Slooff, J. W., 1993, Computational Methods for the Aerodynamic Design of Aircraft Components, *Annual Review of Fluid Mechanics*, vol. 25, pp. 183-214.

- Lane, K. A., and Marshall, D. D., 2010, Inverse Airfoil Design Utilizing CST Parameterization, *48th AIAA Aerospace Sciences Meeting Including the New Horizons Forum and Aerospace Exposition*, Orlando, Florida.
- Leifsson, L., and Koziel, S., 2010, Multi-fidelity design optimization of transonic airfoils using physics-based surrogate modeling and shape-preserving response prediction, *Journal of Computational Science*, vol. 1, no. 2, pp. 98-106.
- Leifsson, L., and Koziel, S., 2011, Inverse Design of Transonic Airfoils Using Variable-Resolution Modeling and Pressure Distribution Alignment, *International Conference on Computational Science*, Singapore, June 1-3.
- Leoviriyakit, K., Kim, S., and Jameson, A., 2003, Viscous Aerodynamic Shape Optimization of Wings including Planform Variables, *21st Applied Aerodynamics Conference*, Orlando, Florida, June 23-26.
- Robinson, T. D., Eldred, M. S., Willcox, K. E., and Haines, R., 2008, Surrogate-Based Optimization Using Multifidelity Models with Variable Parameterization and Corrected Space Mapping, *AIAA Journal*, vol. 46, no. 11.
- Tannehill, J. A., Anderson, D. A., and Pletcher, R. H., 1997, *Computational fluid mechanics and heat transfer*, 2nd edition, Taylor & Francis.
- Queipo, N. V., Haftka, R. T., Shyy, W., Goel, T., Vaidynathan, R., and Tucker, P.K., 2005, Surrogate-Based Analysis and Optimization. *Progress in Aerospace Sciences*, 41(1), pp. 1-28.

PRESS
TECHNOLOGY PUBLICATIONS